

Lattice vibrational modes in changchengite from Raman spectroscopy and first principles electronic structure

B. Chatterjee,¹ D. Vengust,² A. Mrzel,² P.Sutar,² E. Goreshnik,³ J. Mravlje,¹ and T. Mertelj^{2, 4, *}

¹Department of Theoretical Physics, Jozef Stefan Institute, Jamova 39, 1000 Ljubljana, Slovenia

²Department of Complex Matter, Jozef Stefan Institute, Jamova 39, 1000 Ljubljana, Slovenia

³Dept. of Inorganic Chemistry and Technology, Jozef Stefan Institute, Jamova 39, 1000 Ljubljana, Slovenia

⁴Center of Excellence on Nanoscience and Nanotechnology Nanocenter (CENN Nanocenter), Jamova 39, 1000 Ljubljana, Slovenia

(Dated: December 23, 2022)

We measured room-temperature phonon Raman spectra of changchengite (IrBiS) and compared the experimental phonon wavenumbers to the theoretical ones obtained by means of the *ab initio* density-functional-theory calculations in the presence and absence of the spin-orbit coupling effects. Combining two different excitation photon energies all the symmetry predicted Raman modes are experimentally observed. The electronic properties of IrBiS are found to be similar to the recently studied isostructural compound IrBiSe showing a large Dresselhaus spin-orbit valence band splitting. A good agreement between the experimental and theoretically predicted Raman phonon wavenumbers is found only when the lattice parameter is constrained to the experimental value. The inclusion of the spin orbit coupling does not significantly affect the phonon wavenumbers.

Keywords: IrBiS, changchengite, Raman, lattice vibrations, DF theory

I. INTRODUCTION

Changchengite with chemical formula IrBiS is a naturally occurring¹ pyrite (FeS₂) related compound, but was first reported as an artificially synthesized compound² and found to be semiconducting as expected from the chemical similarity to pyrite. Recently, its sister compound IrBiSe has been highlighted for its large spin-orbit splitting resulting in fully spin-polarized valence-band pockets with a peculiar 3D chiral spin texture. It was suggested³ that the presence of such pockets could offer a possibility for generation of electrically controlled spin polarized currents for spintronic applications.

Ab initio calculations⁴ for IrBiSe also suggest a strong bulk photo voltaic effect and a large shift-current. Combination of symmetry analysis and *ab initio* calculations⁵ for IrBiSe further predict a realization of Weyl phonons characterized by Chern number ± 4 .

One expects similar behavior also in IrBiS, however, apart from the initial discovery structural and transport data² and recent ARPES results³ in IrBiSe virtually no other experimental data exist for IrBiS and IrBiSe. Contrary to IrBiSe the electronic structure of IrBiS has not been explored.

In the present study we measured phonon Raman spectra in IrBiS single crystals and compared them to theoretical predictions by *ab initio* density-functional methods taking into account the strong spin-orbit coupling (SOC). At first, neglecting the SOC, we find a decent agreement between the experimental and theoretically calculated Raman phonon wavenumbers. Inclusion of the SOC does not significantly improve the agreement unlike observed in the previous studies in the heavy metals Bi and Pb, where the inclusion of SOC significantly improved the agreement.^{6,7} On the other hand, constraining the lattice parameter to the experimental value further improved the agreement between theory and experiment.

The theoretical electronic band structure of IrBiS is found to be similar to IrBiSe. The reasonably good agreement between the *ab initio* density functional calculations and experimental electronic band structure in IrBiSe by ARPES³ and the experimental lattice dynamics in IrBiS in the present case demonstrate that band-structure calculations work well in this class of compounds and could be used to further explore suitability of related compounds for spintronic applications.

For comparison we also calculated the Brillouin zone center phonon modes of IrBiSe, which agree to those reported in Ref. [5] and are, as expected, softer compared to IrBiS.

The paper is organized as follows: We describe the experimental procedure in Section II and the computational methods in Section III. In Section IV we present and discuss the experimental and theoretical results. Finally, in Section V we summarize and conclude. In Appendix we present our theoretically calculated phonon mode wavenumbers in IrBiSe and compare it to the phonon mode wavenumbers in IrBiS.

II. EXPERIMENTAL

A. Crystal growth and characterization

IrBiS crystallizes in pyrite derived non-centrosymmetric simple cubic crystal structure (space-group P2₁3 (No. 198), point group T (23)) with 4 formula units in the unit cell ($a_{\text{exp}} = 6.143 \text{ \AA}$).² The structure can be viewed as a network of distorted IrBi₃Se₃ octahedra with each Bi or Se ion shared to three such octahedra [see Fig. 1 (a)].

IrBiS crystals were grown unintentionally during growth of thiospinel CuIr₂S₄ single crystals from Bi flux⁹ following the procedure developed in Ref.[10]. In the present case 0.196 g of CuIr₂S₄ powder was mixed with 6.5 g of

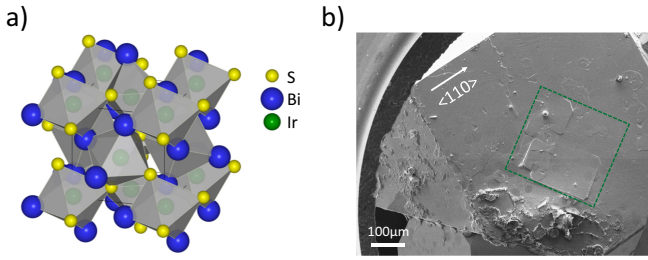


Figure 1. (a) Schematics⁸ of IrBiS cubic $P2_13$ crystal structure. Each Ir ion is coordinated by a combination of three Bi and three S ions forming distorted octahedron. Each of Bi and S ions is shared by three such octahedra. (b) Scanning electron image of the largest crystal. The axes orientation was determined from the morphology and confirmed by the Raman selection rules. Some impurities and a $\sim 45^\circ$ rotated overgrowth (green rectangle) are observed in the bottom part.

Bi and vacuum sealed in a double compartment¹⁰ quartz tube. The tube was put into a furnace programmed to ramp to 1050°C in 24h with a 72h dwell followed by slow cooling of 1.5°C/h to 500°C . At this temperature most of the liquid phase is usually separated from the solid phases by appropriately tilting the tube followed by 12h cooling to a room temperature. The resulting crystals are cleaned of the remaining solidified flux by washing in hot concentrated HNO_3 .

During the crystal growth producing IrBiS crystals the furnace was found to be at room temperature with the program stopped 12 days after the program has started, presumably due to a transient power outage sometime between day 2 and 12 or programming error. The heat treatment procedure was restarted from the beginning using the same sample/quartz tube containing the partially processed solidified melt. After finishing the procedure by washing the product in hot concentrated HNO_3 a clump of a few IrBiS single crystals was recovered instead of the usual CuIr_2S_4 single crystals. Due to the described anomaly during the initial heat treatment run the particular growth conditions for IrBiS single crystals are unfortunately not known in detail and a controlled synthesis/growth of IrBiS single crystals has not been yet achieved.

Single-crystal X-ray diffraction data from the obtained crystals were collected on a Gemini A diffractometer equipped with an Atlas CCD detector, using graphite monochromated Mo-K_α radiation. The collected diffraction data were processed with the CrysAlis PRO program. For unit cell checking 6 runs of 30 frames were collected. The unit cell belonging to the cubic system with the lattice constant $a = 6.14 \text{ \AA}$ was determined using 98 observed reflections. The found unit cell fully corresponds to that found in ICSD database for BiIrS (rec. No. 616740)².

A scanning electron microscope image of the largest

obtained IrBiS crystal is shown in Fig. 1 (b). The crystal shows $\langle 100 \rangle$ and $\langle 111 \rangle$ facets and composition Ir:Bi:S close to 1:1:1 (see Tab. SI (Supporting Information)). Impurities present as chunks on otherwise smooth surfaces are different phases containing also Cu and were not studied in detail.

B. Raman scattering

Room temperature Raman scattering experiments were conducted in a micro-Raman setup (back-scattering configuration) using 632.8 nm and 488 nm excitation using $10\times$ optical objective and $\sim 1 \text{ mW}$ laser power. Possible sample damage due to the laser excitation was checked by measuring a few spectra at lower as well as higher (using $20\times$ and $60\times$ objectives) excitation power densities and no differences or deterioration were observed with increasing excitation power density.

The spectra were collected from as grown $\langle 100 \rangle$ facets where the excitation and detection polarizations were oriented according to the facet edge morphology resulting in systematic mode extinctions as expected from the group theoretical analysis (see also Subsection IV A).

III. COMPUTATIONAL METHODS

We performed electronic structure calculations using the density functional theory (DFT) by means of the pseudo-potential plane-wave Quantum ESPRESSO software package that we also used to perform structural relaxations and to compute the phonon modes at the Γ -point using the density functional perturbation theory (DFPT).¹¹ The basis set cut-off for the plane-wave, and charge density expansion was chosen to be 55 Ry and 440 Ry respectively. The Brillouin zone was sampled on a 6 by 6 by 6 uniform grid according to the Monkhorst-Pack scheme. The threshold parameter¹¹ "tr2_ph" controlling the convergence of the self-consistent calculation of the phonon modes using DFPT was set to 10^{-15} . Calculations performed with a larger threshold parameter resulted in nonphysical/negative phonon wavenumbers due to uncompleted convergence.

The exchange-correlation functional was treated within the generalized gradient approximation (GGA) using Perdew-Burke-Ernzerhof (PBE) functional. The SOC was included using a fully relativistic ultra soft pseudo potential calculated by Dal Corso¹². For the calculations without the SOC we used the ultra-soft non-norm conserving pseudo-potential, with scalar relativistic correction only, from the 'SSSP-1.0-PBE-precision' library¹³.

We performed a structural relaxation such that the forces on each atom in the unit cell were less than 10^{-4} Ry/au , and the total stress was below $2 \times 10^{-7} \text{ Ry/Bohr}^3$. The lattice parameter, $a = 6.213 \text{ \AA}$ (volume of the unit cell $V = 239.80 \text{ \AA}^3$), of the relaxed structure as well as the experimental lattice parameter, $a_{\text{exp}} = 6.143 \text{ \AA}$,

were used for the electronic structure and phonon mode calculations.

We also performed DFT calculations using all-electron, linear augmented plane-wave basis method as implemented in WIEN2k package¹⁴ with the following parameters: the radii of the muffin-tin spheres were $R_{\text{MT}}(\text{Bi}) = 2.5 a_{\text{B}}$ for bismuth atoms and $R_{\text{MT}}(\text{Ir}) = 2.5 a_{\text{B}}$ for iridium atoms, and $R_{\text{MT}}(\text{S}) = 2.0 a_{\text{B}}$ for sulfur atoms. The Brillouin zone was sampled with 10000 k points (451 k points in the irreducible wedge) in the self-consistent cycle. The basis-set cutoff K_{max} was defined with $R_{\text{MT}}(\text{Bi}) \times K_{\text{max}} = 7.0$. Scalar relativistic effects as well as the SOC on a second variational level were included. The band structures obtained from the Quantum ESPRESSO and WIEN2k packages are consistent. The band structure plots shown in the present paper were calculated using the WIEN2k package.

IV. RESULTS AND DISCUSSIONS

A. Raman scattering

Optical modes for IrBiS with non-centrosymmetric space group $P2_13$ are classified according to the irreducible representations of point group $T(23)$ as¹⁵ $\Gamma_{\text{optic}} = 3A + 3^1E + 3^2E + 8T$. The label A refers to the non degenerate totally symmetric representation. 1E and 2E are one dimensional complex conjugate representations that correspond to two degenerate (due to the time reversal symmetry) modes. T refers to a triply degenerate representation. All optical modes are Raman active¹⁵ while only the T modes are infrared active. Since the symmetries of all three atomic sites are identical the modes of each symmetry come in multiples of 3, where one of the 9T triply degenerate groups corresponds to the acoustic branches.

To assign the observed modes symmetry we search for systematic extinctions as a function of the relative orientations between the excitation light, the detection analyzer polarizations and the crystal orientation (in the back-scattering geometry). The A modes Raman tensor¹⁵ is diagonal and isotropic with $\chi_{xx} = \chi_{yy} = \chi_{zz}$. The A modes are therefore extinct in the crossed polarizations configuration (CPC) irrespective of the crystal orientation. The two E modes Raman tensors are also diagonal, but anisotropic, $\chi_{xx} \neq \chi_{yy} \neq \chi_{zz}$.² When the excitation polarization is parallel to the $\langle 100 \rangle$ directions the scattered light polarization is parallel to the excitation one, so the modes are extinct in the CPC, while for a general crystal orientation the observation is allowed in both, the CPC and the parallel polarization configuration (PPC). The T modes Raman tensors are purely off-diagonal and symmetric³ with $\chi_{yz} = \chi_{xz} = \chi_{xy}$. As a result, the T modes are extinct in the PPC when the excitation polarization is parallel to the $\langle 100 \rangle$ directions and in the CPC when the excitation polarization is parallel to the $\langle 110 \rangle$ directions.

Taking the $z(x, x)$ - z scattering geometry⁴ the T modes must be systematically extinct, while the A and E modes must be systematically extinct in the $z(x, y)$ - z scattering geometry. To separate out the E modes the $z(x', y')$ - z , with $x' = x + y$ and $y' = x - y$, scattering geometry is instrumental since both, the A and T modes must be extinct.

In Fig. 2 we show experimental polarized Raman spectra. The relative intensities of most of the modes are quite different comparing the two excitation wavelengths indicating the presence resonant Raman effects. This is expected since both excitation photon energies are well above the gap.

Combining the spectra at both laser excitation wavelengths we observe all the symmetry-predicted optical modes where the T modes at 148.5 cm^{-1} and 320.9 cm^{-1} are observable only at a single laser wavelength. The lowest wavenumber (84.4 cm^{-1}) A mode is also missing at 488-nm excitation presumably due to its wavenumber being at the very edge of the 488-nm laser-rejection filter window. Taking the morphologically determined crystal orientation all the expected mode extinctions are observed. The wavenumbers and symmetries of all modes are compiled in Tab. I.

We observe a separate group of peaks ($1A + 1^{1,2}E + 3T$) above 300 cm^{-1} , which can be associated with the modes dominated by the lightest S ions displacements. On the other hand, the other modes observed below 200 cm^{-1} appear as a single group. Since the masses of Ir and Bi are very similar these modes are expected to have mixed displacements. Nevertheless, the progression of the mode symmetries still reflects the mechanical-representation structure, where each atomic site generates ($1A + 1^{1,2}E + 3T$) representations.⁵

B. Electronic band structure

In Fig. 3 we present a comparison of the electronic band structure without (a) and with (b) SOC using the relaxed lattice parameters. A clean band-gap appears across the Fermi level indicating that IrBiS is a band-insulator/semiconductor. We find an overall agreement of the band structure³ and the SOC induced effects on the bands with the related isostructural compound IrBiSe.

As in the Se compound we observe a large $\sim 0.34 \text{ eV}$ splitting of the top-most valence band (in red) due to the SOC where the hole pockets would appear upon light hole doping (indicated by a dotted line with double headed arrow in Fig. 3 (b)). These bands have predominantly Ir- d character (see Fig. 4). The splitting vanishes at the time reversal symmetry points and the Brillouin zone (BZ) boundaries and is almost negligible along the BZ diagonal (Γ -R). The splitting also decreases as we move away from the Fermi level.

The splitting *at the top* of the valence band in IrBiS is one order of magnitude larger than that observed *at the top* of the valence band^{20,21} in GaAs.⁶ The valence band

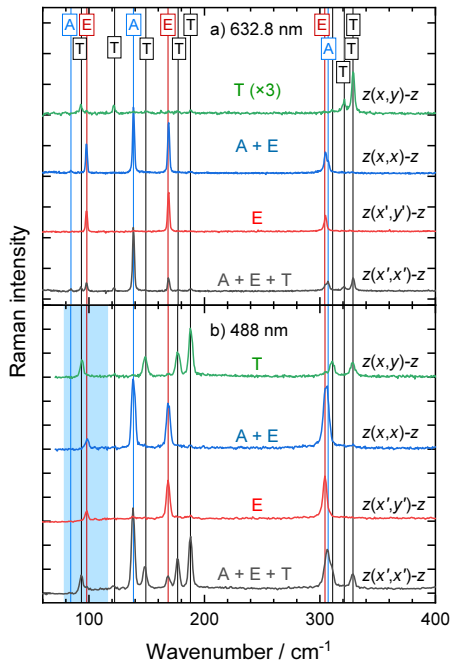


Figure 2. Measured Raman spectra in different scattering geometries a) and b) with 632.8 nm and 488 nm excitation, respectively. Porto notation is used with $x' = x + y$ and $y' = x - y$. The lines in b) appear broader due to a worse instrumental resolution at 488 nm. The blue shaded region in b) corresponds to the region where the sensitivity strongly drops with decreasing wavenumber due to the 488-nm edge filter.

pockets in IrBiS are therefore, similarly to IrBiSe³, fully spin polarized as shown by the arrows in Fig. 5.

While the intrapocket (intravalley) scattering should not be strongly affected due to the spin polarization the inter-pocket (intervalley) scattering is expected to be partially suppressed and anisotropic. Each pocket has one corresponding pocket at the opposite momentum with exactly the opposite spin polarization (due to the time reversal symmetry), one pocket with nearly anti-parallel spin polarization, one pocket with nearly parallel spin polarization and 8 pockets with approximately perpendicular spin polarization. This could have profound effects on spin relaxation and spin transport properties, however, the detailed analysis of these effects is beyond the scope of the present paper.

C. Lattice vibrational modes and Raman spectra

The calculated lattice parameters and the internal atomic parameters obtained using the GGA functional are presented in Table II while Table I shows the phonon wavenumbers calculated at the Brillouin zone Γ point. The phonon modes symmetries according to the point group symmetry T(23) are also indicated.

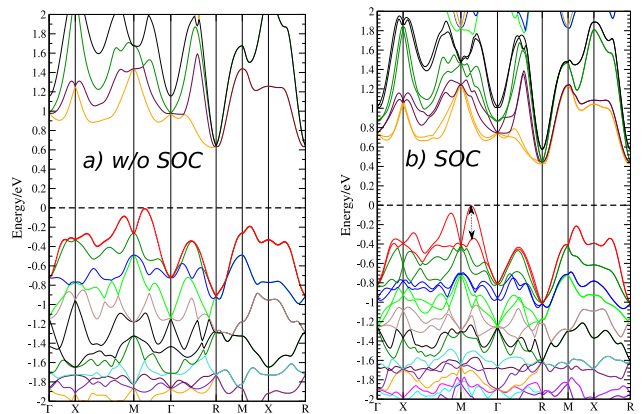


Figure 3. The electronic band-structure of IrBiS without (a) and with (b) SOC from the Wien2k calculations using GGA. The dotted line with a double-headed arrow indicates the large valence band (~ 0.34 -eV) Dresselhaus splitting due to the SOC. The dashed line at 0 eV corresponds to the ($T = 0$ K) Fermi level.

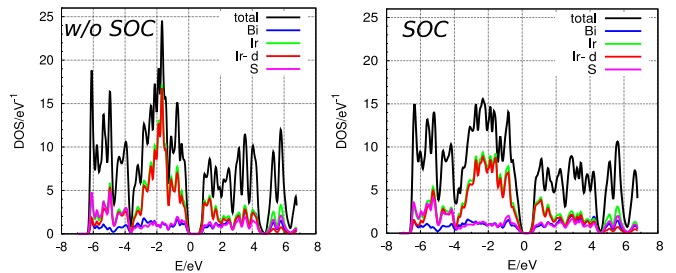


Figure 4. The total and partial density of states in IrBiS without (left) and with (right) SOC from the Wien2k calculations using GGA. Explicitly we show the the Bi, Ir, S, and orbital resolved d states for Ir.

The mode wavenumbers calculated using the relaxed lattice parameter, $a = 6.213$ Å, which is larger than the experimental, $a_{\text{exp}} = 6.143$ Å, appear significantly softer than the experimental ones. The inclusion of SOC hardens most of the modes, but not significantly, so the resulting wavenumbers remain $\sim 5\%$ to $\sim 11\%$ softer than the experimental ones. The effect of SOC is the largest for the three modes calculated to be around ~ 290 cm⁻¹. The calculated⁷ 294.4 cm⁻¹ A mode softens by 1.9% while the 275.9 cm⁻¹ E mode and the 282.6 cm⁻¹ T mode harden by 3.5% and 2.9%, respectively. All these modes are S ions displacements dominated (see Table SII (Supporting Information)). Experimentally these modes lay between 305 cm⁻¹ (the E mode) and 311 cm⁻¹ (the T mode) with the T mode being harder than A, contrary to the calculations.

Taking the smaller experimental lattice parameter hardens the modes bringing most of the wavenumbers within a 3% discrepancy band with most of the modes remaining

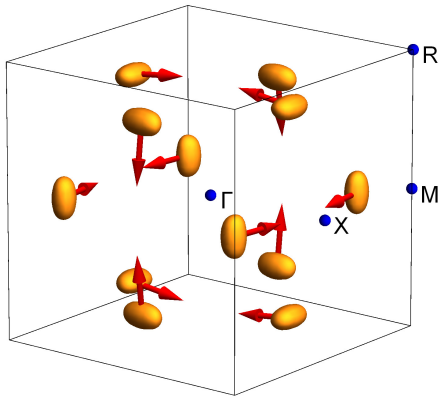


Figure 5. Hole pockets corresponding to the highest valence band. The direction of spin in different pockets is indicated by the red arrows.

too soft. The inclusion of SOC slightly improves match for most of the modes, however, the calculated⁸ 331.7 cm^{-1} T mode wavenumber and the 306.9 cm^{-1} A mode wavenumber are significantly closer to the experimental wavenumbers in the absence of SOC. In both cases they fall well within the 3% discrepancy band.

There are still a few modes that show discrepancies in excess of 3% even after inclusion of the SOC: the calculated⁹ 84 cm^{-1} A mode, the 87.1 cm^{-1} T mode, and the T mode pair at 165.9 cm^{-1} and 178.1 cm^{-1} . These modes show the largest discrepancies also with the relaxed lattice parameter. Looking at the order of modes, the highest wavenumber A mode is pushed below the highest wavenumber E mode, contrary to what is observed in the experiment.

It will be interesting to explore in future work whether going beyond the pseudo-potential plane wave method and using the full potential augmented plane wave method or using more advanced functionals to treat the exchange

correlation effects within the DFT would improve the agreement.

For comparison we also computed the phonon modes at the Γ -point in IrBiSe and found them to be systematically softer than in IrBiS. The details are presented in Supporting Information.

V. SUMMARY AND CONCLUSIONS

We measured phonon Raman spectra in IrBiS, a semiconductor which displays a large bulk-type Dresselhaus valence bands splitting of $\sim 0.3\text{ eV}$, and compared the experimental phonon wavenumbers to the *ab initio* predicted ones by taking into account the SOC effects.

Using two different excitation wavelengths all the symmetry predicted phonon modes were experimentally observed. The calculated wavenumbers appear systematically softer than the experimental ones. The inclusion of SOC shows mostly a minor hardening of the phonon wavenumbers in comparison to the lattice parameter effects, where constraining the lattice parameter to the smaller experimental value hardens most of the calculated phonon wavenumbers within a 3% discrepancy band.

Comparing the phonon mode wavenumbers of the sister compound IrBiSe to IrBiS we find a strong, $\sim 35\%$, softening of the chalcogen-displacements dominated modes and a lesser, $\sim 4\%$, softening of the Ir/Bi-displacements dominated modes.

The calculated electronic structure of IrBiS is found to be similar to the sister compound IrBiSe with almost fully spin polarized valence-band hole pockets.

ACKNOWLEDGMENTS

The authors acknowledge the financial support of Slovenian Research Agency (research core funding No-P1-0040 and P1-0044 and research project funding J1-2458) for financial support.

* tomaz.mertelj@ijs.si

¹ Y. Zuxiang, *Acta Geol. Sin. (Engl. Ed.)* **1997**; *71*, 486.

² F. Hulliger, *Nature* **1963**; *198*, 382.

³ Z. Liu, S. Thirupathiah, A. N. Yaresko, S. Kushwaha, Q. Gibson, W. Xia, Y. Guo, D. Shen, R. J. Cava, S. V. Borisenko, *Phys. Status Solidi RRL* **2020**; *14*, 1900684.

⁴ Y. Zhang, F. de Juan, A. G. Grushin, C. Felser, Y. Sun, *Phys. Rev. B* **2019**; *100*, 245206.

⁵ Q.-B. Liu, Z. Wang, H.-H. Fu, *Phys. Rev. B* **2021**; *103*, L161303.

⁶ L. Díaz-Sánchez, A. Romero, X. Gonze, *Phys. Rev. B* **2007**; *76*, 104302.

⁷ M. J. Verstraete, M. Torrent, F. Jollet, G. Zérah, X. Gonze, *Phys. Rev. B* **2008**; *78*, 045119.

⁸ K. Momma, F. Izumi, *J. Appl. Crystallogr.* **2011**; *44*, 1272.

⁹ M. Naseska, P. Sutar, D. Vengust, S. Tsuchiya, M. Čeh, D. Mihailovic, T. Mertelj, *Phys. Rev. B* **2020**; *101*, 165134.

¹⁰ N. Matsumoto, S. Nagata, *J. Cryst. Growth* **2000**; *210*, 772.

¹¹ P. Giannozzi, O. Andreussi, T. Brumme, O. Bunau, M. B. Nardelli, M. Calandra, R. Car, C. Cavazzoni, D. Ceresoli, M. Cococcioni, *et al.*, *J. Phys.: Condens. Matter* **2017**; *29*, 465901.

¹² A. Dal Corso, *Comput. Mater. Sci.* **2014**; *95*, 337.

¹³ G. Prandini, A. Marrazzo, I. E. Castelli, N. Mounet, E. Passaro, N. Marzari, *Materials Cloud Archive* **2021**; *2021.76*.

¹⁴ P. Blaha, K. Schwarz, F. Tran, R. Laskowski, G. K. Madsen, L. D. Marks, *J. Chem. Phys.* **2020**; *152*, 074101.

¹⁵ E. Kroumova, M. Aroyo, J. Perez-Mato, A. Kirov, C. Capillas, S. Ivantchev, H. Wondratschek, *Phase Transitions*

- 2003; 76, 155.
- ¹⁶ $\chi_{zz} = 0$ for the 2E modes.
- ¹⁷ Assuming the absence of strong resonant effects.
- ¹⁸ In Porto notation.
- ¹⁹ In the lowest wavenumber group the 3T acoustic modes are not visible in Raman spectra.
- ²⁰ S. Cho, W. Jung, J. Hong, B. Kim, G. Han, M. Leandersson, T. Balasubramanian, M. Arita, K. Shimada, J. H. Shim, *et al.*, *Curr. Appl. Phys.* **2021**; 30, 96.
- ²¹ I. Drichko, I. Y. Smirnov, A. Suslov, K. Baldwin, L. Pfeiffer, K. West, *Phys. Rev. B* **2021**; 104, 155302.
- ²² The maximal SOC splitting of the valence bands in GaAs and IrBiS are of comparable magnitude, however, unlike to IrBiS, where the top of the valence band is at the low symmetry point, the top of the valence bands in GaAs is at the Γ point where the splitting vanishes due to the symmetry.
- ²³ Without SOC.
- ²⁴ Without SOC.
- ²⁵ With SOC.
- ²⁶ $\chi_{zz} = 0$ for the 2E modes.
- ²⁷ Assuming the absence of strong resonant effects.
- ²⁸ In Porto notation.
- ²⁹ In the lowest wavenumber group the 3T acoustic modes are not visible in Raman spectra.
- ³⁰ The maximal SOC splitting of the valence bands in GaAs and IrBiS are of comparable magnitude, however, unlike to IrBiS, where the top of the valence band is at the low symmetry point, the top of the valence bands in GaAs is at the Γ point where the splitting vanishes due to the symmetry.
- ³¹ Without SOC.
- ³² Without SOC.
- ³³ With SOC.
- ³⁴ The complex E representations are from the point of view of the spatial symmetry one dimensional.
-

Table I. Comparison between experimental and calculated phonon wavenumbers of at the Γ -point in IrBiS without and with SOC using the ultra-soft non-norm conserving GGA pseudo potential.

Experimental		Calculations (relaxed, $a = 6.213 \text{ \AA}$)			Calculations (constr., $a_{\text{exp}} = 6.143 \text{ \AA}$)			Symmetry	Activity
632.8 nm	488 nm	without SOC	with SOC	Δ^a	without SOC	with SOC	Δ^b		
Wavenumber (cm^{-1})					Wavenumber (cm^{-1})				
-	-	-0.20	0.0	-	0.0	0.0	-	T	acoustic
84.4	-	79.04	78.4	-7.1	81.4	81.3	-3.7	A	R
93.0	93.7	83.8	84.8	-9.2	86.2	87.1	-6.7	T	I+R
97.9	98.2	91.2	92.6	-5.6	95.1	96.4	-1.7	E	R
121.6	122.0	114.1	113.7	-6.7	118.4	118.3	-2.9	T	I+R
138.6	138.4	127.6	127.5	-7.9	134.4	134.9	-2.6	A	R
-	148.5	133.1	135.1	-9.0	142.2	145.0	-2.4	T	I+R
169.0	168.7	154.1	155.5	-7.9	163.0	164.4	-2.6	E	R
177.1	176.9	156.2	157.4	-11.1	164.4	165.9	-6.3	T	I+R
188.1	188.0	165.9	167.2	-11.1	176.4	178.1	-5.3	T	I+R
304.8	305.4	275.9	285.6	-6.4	300.1	310.0	1.6	E	R
307.5	307.0	294.4	288.8	-6.0	306.9	301.8	-1.8	A	R
311.2	310.7	282.6	290.7	-6.5	306.3	313.8	0.9	T	I+R
320.9	-	300.8	302.9	-5.6	321.1	319.6	-0.4	T	I+R
328.8	328.3	314.2	312.8	-4.8	331.7	335.1	2.0	T	I+R

^a Using the theoretical results with the relaxed lattice constant and SOC.

^b Using the theoretical results with the experimental lattice constant and SOC.

Table II. Calculated internal atomic parameters of IrBiS after a complete structural relaxation using the PBE functional (without SOC) for the relaxed lattice parameter, $a = 6.213 \text{ \AA}$, and the constrained lattice parameter, $a = 6.143 \text{ \AA}$ (experimental lattice constant) compared to the experimental atomic positions as reported in Ref. [2]. These parameters remain similar also after the inclusion of SOC (not shown).

atom	site ($P2_13$)	$x=y=z$ ^a	$x=y=z$ ^b	$x=y=z$ ^c
Bi	4a	0.370	0.369	0.39
Ir	4a	0.024	0.025	0.02
S	4a	0.617	0.617	0.615

^a $a = 6.213 \text{ \AA}$

^b $a = 6.143 \text{ \AA}$

^c expt, Ref.²

Supplementary Information: Lattice vibrational modes in changchengite from Raman spectroscopy and first principles electronic structure

B. Chatterjee¹, D. Vengust², A. Mrzel², P. Sutar², E. Goreshnik³, J. Mravlje¹, and T. Mertelj^{2,4}

¹*Department of Theoretical Physics, Jozef Stefan Institute, Jamova 39, 1000 Ljubljana, Slovenia*

²*Department of Complex Matter, Jozef Stefan Institute, Jamova 39, 1000 Ljubljana, Slovenia*

³*Dept. of Inorganic Chemistry and Technology, Jozef Stefan Institute, Jamova 39, 1000 Ljubljana, Slovenia*

⁴*Center of Excellence on Nanoscience and Nanotechnology Nanocenter (CENN Nanocenter), Jamova 39, 1000 Ljubljana, Slovenia*

VI. CRYSTAL CHARACTERIZATION

The results of from Energy-dispersive X-ray spectroscopy analysis of different IrBiS crystals composition are shown in Table III. Within the expected accuracy of the technique the composition Ir:Bi:S is 1:1:1.

VII. SOC CALCULATIONS TREATING THE BI 6P-1/2 STATE WITH LOCAL ORBITAL

To improve the description of the heavy elements $6p$ states one can include the local orbitals (LO) as described in Ref.¹. This was not included in the SOC results shown in the main paper, however, to estimate the possible improvement of the calculations we performed some calculations including the LO as well. A comparison of the band structure when adding the heavier Bi atom LO shows no qualitative and only negligible quantitative differences in the over all band-structure as shown in Fig. 6(left). The SOC splitting of the top-most valence band is not at all affected after inclusion of the LO. This is in agreement with the overall chemistry of this compound where the states near the Fermi energy are dominated by the Ir d derived states. The other dominant characters are the S p states and Bi p states with the S p having higher contribution on the occupied side, and the Bi p on the unoccupied side. Hence, the topmost valence band with the dominant Ir d character is not at all affected by adding Bi $6p_{1/2}$ LO.

We have further computed the band structure also adding the Ir $6p_{1/2}$ LO which also show just minor quantitative changes in the band structure as shown in Fig. 6 (right).

VIII. LATTICE VIBRATIONAL MODE DISPLACEMENTS IN IrBiS

In Table IV we show calculated relative phonon displacements magnitudes for each ionic species for the best agreement case of constraining the lattice parameter to the experimental value. Since for each species all sites are crystallographically equivalent the displacement magnitudes must be equal across the species for a single $q = 0$ mode for the A and E symmetry modes¹⁰. For the T symmetry modes the 4 symmetry equivalent unit cell sites can have different displacement magnitudes so the range is given where appropriate.

The high-frequency modes group is clearly S-ion displacements dominated while the low frequency group shows rather mixed displacements with somewhat larger contribution of the heaviest Bi ions in the four lowest wavenumber modes.

The effect of the SOC inclusion on the relative wavenumber shift is the largest for three S-ion-displacements dominated modes and the 145 cm^{-1} -mode that shows the largest relative Ir ion displacements. The reason for this is not understood as the displacements of the modes are rather complex and nonintuitive, due to the low-symmetry distribution of the atoms within the unit cell.

The modes that show frequency discrepancies are all mixed modes and do not show any outstanding relative displacement magnitudes pattern.

IX. Γ -POINT PHONON MODES IN IrBiSe

For comparison we also calculated the phonon mode wavenumbers at the Γ -point (in the absence of SOC) in the sister compound IrBiSe. We used similar settings and method like in the case of IrBiS. In Tab. V we present the

phonon mode wavenumbers in IrBiSe for a completely relaxed structure with the relaxed lattice constant of $a = 6.38$ Å, which is, similar as in IrBiS, found larger than the experimental,² $a_{\text{exp}} = 6.290$ Å.

There is an overall softening of the mode wavenumbers as compared to IrBiS. While the low wavenumber modes (below ~ 160 cm^{-1}) are softer only by ~ 5 %, the high wavenumber Se modes (above ~ 190 cm^{-1}) are significantly softer by ~ 35 %. The wavenumber of the doubly degenerate charge four Weyl phonon mode at 87.8 cm^{-1} (2.633 THz) is consistent with the results presented in Ref. [5]. The corresponding doubly degenerate mode in IrBiS is found at 91.2 cm^{-1} . It could be an interesting future work to study the complete phonon dispersion in IrBiS and further investigate the Weyl phonons.

* tomaz.mertelj@ijs.si

¹ J. Kunes, P. Novak, R. Schmid, P. Blaha, and K. Schwarz, *Phys. Rev. B.* **2001**; *64*, 153102.

² $\chi_{zz} = 0$ for the ²E modes.

³ Assuming the absence of strong resonant effects.

⁴ In Porto notation.

⁵ In the lowest wavenumber group the 3T acoustic modes are not visible in Raman spectra.

⁶ The maximal SOC splitting of the valence bands in GaAs and IrBiS are of comparable magnitude, however, unlike to IrBiS, where the top of the valence band is at the low symmetry point, the top of the valence bands in GaAs is at the Γ point where the splitting vanishes due to the symmetry.

⁷ Without SOC.

⁸ Without SOC.

⁹ With SOC.

¹⁰ The complex E representations are from the point of view of the spatial symmetry one dimensional.

Table III. Composition of different crystals obtained from Energy-dispersive X-ray spectroscopy.

No.	Ir (at. %)	Bi (at. %)	S (at. %)
1.	32.8	33.5	33.8
2.	33.7	32.7	34.0
3.	31.0	33.6	35.4
4.	32.3	33.9	33.8

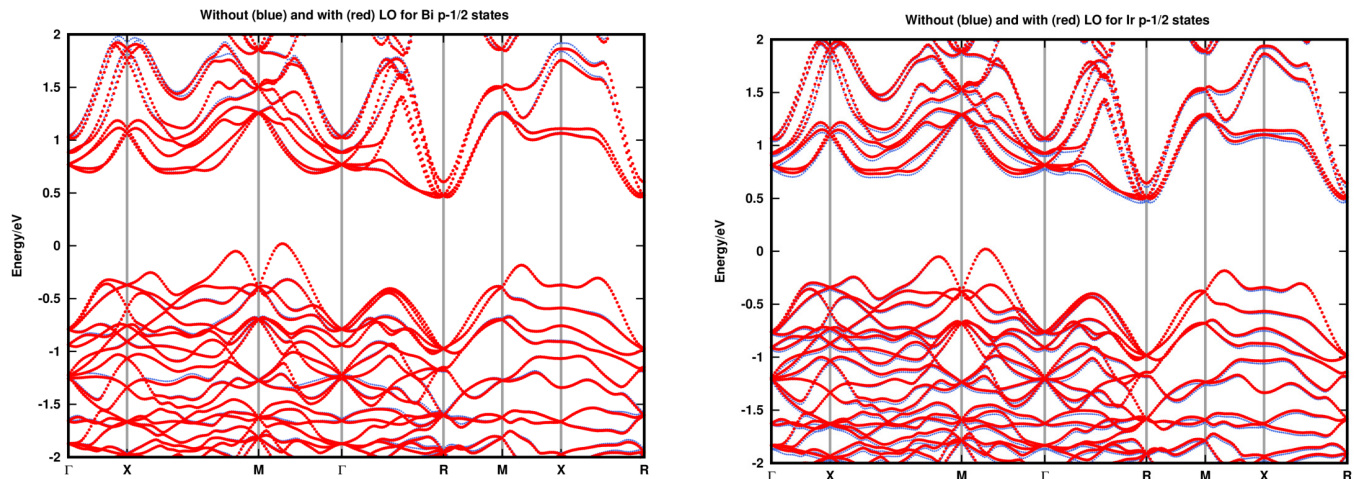
Figure 6. Left: Bi $6p_{1/2}$ states treated with LO (red) and without LO (blue). Right: Ir $6p_{1/2}$ states treated with LO (red) and without LO (blue).

Table IV. Calculated ionic phonon displacements magnitudes for the best agreement case of using the experimental lattice parameter. A range is given (see text) for the T symmetry modes where appropriate. The modes that show frequency discrepancies in excess of 3% are shown in magenta.

Experimental 632.8 nm	488 nm	Calculations		Symmetry	Displacement magnitude ^a					
		$a = a_{\text{exp}}$ ^b	Δ_{SOC} ^c		without SOC			with SOC		
Wavenumber (cm ⁻¹)			%	-	Ir	Bi	S	Ir	Bi	S
84.4	-	81.3	-0.1	A	0.49	1.00	0.51	0.47	1.00	0.49
93.0	93.7	87.1	1.0	T	0.74 - 0.83	0.81 - 1.00	0.59 - 0.66	0.74 - 0.81	0.83 - 1.00	0.59 - 0.65
97.9	98.2	96.4	1.4	E	0.94	1.00	0.34	0.92	1.00	0.34
121.6	122.0	118.3	-0.1	T	0.48 - 0.51	0.82 - 1.00	0.12 - 0.18	0.48 - 0.51	0.81 - 1.00	0.10 - 0.15
138.6	138.4	134.9	0.4	A	1.00	0.45	0.04	1.00	0.44	0.08
-	148.5	145.0	2.0	T	0.79 - 1.00	0.22 - 0.38	0.11 - 0.19	0.75 - 1.00	0.21 - 0.41	0.06 - 0.18
169.0	168.7	164.4	0.9	E	1.00	0.90	0.66	1.00	0.88	0.70
177.1	176.9	165.9	0.9	T	0.34 - 1.00	0.38 - 0.97	0.27 - 0.60	0.44 - 1.00	0.46 - 0.98	0.33 - 0.63
188.1	188.0	178.1	1.0	T	0.64 - 1.00	0.70 - 0.94	0.17 - 0.21	0.67 - 1.00	0.71 - 0.94	0.18 - 0.21
304.8	305.4	310.0	3.3	E	0.09	0.03	1.00	0.09	0.03	1.00
307.5	307.0	301.8	-1.7	A	0.04	0.06	1.00	0.04	0.06	1.00
311.2	310.7	313.8	2.4	T	0.08 - 0.11	0.02	0.40 - 1.00	0.08 - 0.09	0.02 - 0.03	0.84 - 1.00
320.9	-	319.6	-0.5	T	0.05	0.02 - 0.05	0.68 - 1.00	0.08	0.03 - 0.07	0.66 - 1.00
328.8	328.3	335.1	1.0	T	0.05	0.06 - 0.08	0.94 - 1.00	0.05	0.04 - 0.05	0.74 - 1.00

^a Relative to the species with the maximum displacement for the given mode.^b with SOC^c Relative shift due to the SOC.

Table V. Calculated phonon wavenumbers at the Γ -point in the sister compound IrBiSe without SOC for the fully relaxed structure with the theoretical lattice constant, $a = 6.38 \text{ \AA}$.

IrBiS	IrBiSe		
Wavenumber (cm^{-1})		Symmetry	Activity
-0.20	0.0	T	I+R
79.04	75.43	A	R
83.8	78.24	T	I+R
91.2	87.8	E	R
114.1	110.5	T	I+R
127.6	124.5	A	R
133.1	130.45	T	I+R
154.1	140.81	E	R
156.2	145.8	T	I+R
165.9	158.5	T	I+R
275.9	189.8	E	R
294.4	184.5	A	R
282.6	191.3	T	I+R
300.8	199.4	T	I+R
314.2	204.4	T	I+R

S/Se dominated